A Parametric Study of Accelerated Carbonation in Alkali-activated Slag

Eric R. McCaslin[1,2], Claire E. White[2,3*]

[1]Department of Chemical and Biological Engineering, Princeton University, Princeton, NJ, 08544, USA

[2]Andlinger Center for Energy and the Environment, Princeton University, Princeton, NJ, 08544, USA

[3]Department of Civil and Environmental Engineering, Princeton University, Princeton, NJ, 08544, USA

* Corresponding author: Phone: +1 609 258 6263, Fax: +1 609 258 2799, Email: whitece@princeton.edu

Postal address: Department of Civil and Environmental Engineering, Princeton University, Princeton NJ 08544, USA

Keywords: Alkali-activated slag, accelerated carbonation, amorphous calcium carbonate, X-ray diffraction, Fourier transform infrared spectroscopy, thermogravimetric analysis

Abstract

Resistance to carbonation is one important attribute that low-CO_2 cement alternatives must possess, and is particularly crucial for cement alternatives subjected to aggressive CO_2 concentrations such as those used in construction of oil wells and wells for below ground carbon sequestration. Here, a parametric study of alkali-activated slag (AAS) carbonation in aggressive environments has been conducted to examine (i) calcium carbonate polymorphism using X-ray diffraction (XRD) and Fourier-transform infrared (FTIR) spectroscopy, and (i) the extent of calcium carbonate formation and CO_2 adsorption using thermogravimetric analysis (TGA). A range of AASs have been studied by varying the magnesium content of the slag, the activator type (sodium hydroxide and sodium silicate), the activator concentration, and the curing time prior to carbonation. It was uncovered that both (i) magnesium from the slag and (ii) silica from the activating solution are needed to reduce the propensity for the sodium-containing calcium-alumino-silicate-hydrate gel to undergo decalcification.

Introduction

Concrete is utilized more extensively around the world on a volume basis than any other engineered material because of its vital role in construction. However, the production of ordinary Portland cement (OPC) powder, the key constituent in concrete, accounts for approximately 5-8% of all anthropogenic CO_2 emissions.[1,2] Among the sustainable alternatives being explored as viable replacements for OPC concrete, alkali-activated materials (AAMs) have emerged as key contenders, especially due to the large-scale case studies around the world demonstrating their performance.[3] AAMs are manufactured by utilization of industrial by-products (such as blast furnace slag and coal-derived fly ash) or thermally treated clays (such as metakaolin) and an alkali activation process, whereby the aluminosilicate-rich precursor powders dissolve in the highly alkaline environment, leading to precipitation of a mechanically-hard binder gel.[3] The macroscopic properties and microstructure of AAMs have been extensively characterized in the past,[3–9] however uncertainties remain regarding long-term in-field performance which can be addressed by discovering the underlying chemistry and physics controlling chemical and/or physical degradation processes.

Carbonation is one of the main chemical degradation mechanisms of both AAM and OPC concrete. From a chemistry perspective, OPC resists carbonation because it contains portlandite, which buffers the pH of the pore solution at ~12.5.[10] However, once all the portlandite has dissolved, carbonation will lead to a lowering of the pore solution pH and therefore irreversible corrosion of any reinforcing steel along with degradation of the main strength-giving phase, calcium-silicate-hydrate (C-S-H gel).[11] In addition to the buffering effects of portlandite, it is also known that carbonation can be mitigated via the development of concrete with low permeability.[12] It has been shown that alkali-activated slag (AAS) pastes and mortars lose strength due to carbonation, specifically for certain accelerated testing conditions where OPC performs favorably.[13–15] However, as outlined by Bernal *et al.*, accelerated carbonation tests that are routinely used to determine the carbonation resistance of OPC severely underestimate the service life of AAS,[16] and the magnesium content of slag has been shown mitigate the extent of carbonation.[17–19]

It has been demonstrated that alkali activation of slag with a significant magnesium content leads to the formation of a hydrotalcite-like phase (a layered double hydroxide (LDH)).[4,5,16,17] Hydrotalcite and other Mg-Al LDH phases consist of magnesium and aluminum layers with hydroxide groups on their surface. In between these layers are charge balancing anions, typically carbonates.[20] The carbonates in the LDH interlayer have been shown to rapidly exchange with CO_2 in the air, and hydrotalcite can also preferentially adsorb CO_2.[21] Some studies on the carbonation of AAS attribute its carbonation resistance to this ability of the hydrotalcite-like LDH phase to act as a CO_2 sink. Bernal *et al.* discovered that during accelerated carbonation of AAS containing MgO, the carbonation depth decreased with increasing MgO content,[17] where they attributed this behavior to greater amounts of the hydrotalcite-like LDH phase. In another study, the presence of high concentrations of sodium silicate was found to suppress the formation of the hydrotalcite-like LDH phase (as determined using X-ray diffraction (XRD)), and correspondingly increase the susceptibility of AAS to carbonation.[18] However, in contrast to this finding Myers *et al.* showed, using thermodynamic modeling, that the hydrotalcite-like LDH phase does extensively precipitate in sodium silicate-activated slag[22]. Additional evidence of this phase in sodium silicate-activated slag has been obtained using scanning electron microscopy - energy dispersive X-ray spectroscopy (SEM-EDX), where the data revealed a fine intermixing of a hydrotalcite-like LDH phase with sodium-containing calcium-alumino-silicate-hydrate (C-(N)-A-S-H) gel.[5] Hence, complementary

experimental techniques, in addition to XRD, are required to accurately determine the phase composition of AAMs.[5,23–25]

There are several industries where cements are exposed to elevated CO_2 concentrations, including cements used in wells for oil and gas operations and CO_2 sequestration.[26] Hence, the behavior of sustainable cements, such as AAS, in such situations is an emerging area of research, where the early-age carbonation behavior of cement-based materials is imperative to understand. In our recent investigation of accelerated carbonation of AAS we used pair distribution function (PDF) analysis to study *in situ* the carbonation mechanism.[27] We found the possible existence of an amorphous calcium carbonate (ACC) that forms during carbonation of 24 hr old AAS paste in 100% CO_2. Slag with higher magnesium content was associated with a greater amount of ACC and a lower extent of degradation of the C-(N)-A-S-H gel (main strength-giving phase). Therefore, it appears that ACC plays a role in mitigating carbonation under accelerated conditions, and that magnesium may stabilize ACC.[28,29] Specifically, due to the metastability of AAC under ordinary conditions, it has a higher solubility than the crystalline calcium carbonate phases that normally form. Thus, the presence of ACC maintains a higher calcium concentration in the pore solution, decreasing the driving force for decalcification of the C-(N)-A-S-H gel. If this is true, then it may be possible to design highly carbonation resistant cements by doping with magnesium, leading to cements that perform favorably in high CO_2 environments such as oil wells and during carbon sequestration.

In this study we explore the influence of two levels of accelerated carbonation (exposure to 5 and 100% CO_2) on carbonate polymorph formation and CO_2 uptake by hydrotalcite-like LDH versus C-(N)-A-S-H gel decalcification (CO_2 uptake studied for 5% CO_2). By employing XRD and Fourier transform infrared spectroscopy (FTIR) we determine how the different parameters used in preparing AAS samples affect the phases that form during carbonation. Moreover, thermogravimetric analysis is used to understand how the MgO content affects the kinetics of the carbonation reaction together with a qualitative assessment of CO_2 uptake by hydrotalcite-like LDH versus carbonate formation (carbonates linked primarily to gel decalcification). From these data we draw conclusions regarding the susceptibility of AAS to suffer degradation when exposed to different CO_2 environments, and how the slag and activator chemistry can be augmented to

reduce the detrimental effects of CO_2 exposure. Finally, we present an updated mechanism which we believe is responsible for the increase carbonation resistance of certain AASs when exposed to elevated CO_2 conditions.

Materials and Methods

Two different sources of blast furnace slag were used with a high and low MgO content. These slags were characterized in a previous study, and their compositions, determined by X-ray fluorescence spectroscopy (XRF), are shown in Table 1.[19] The slags were activated using either a sodium silicate (prepared using anhydrous sodium metasilicate, Na_2SiO_3, Sigma-Aldrich, reagent grade) or sodium hydroxide (NaOH, Sigma Aldrich, reagent grade) solution, each synthesized using deionized water, where an allotted amount of solid material (sodium metasilicate or sodium hydroxide) was dissolved in the water. After the sodium metasilicate was added to deionized water it was left to mix using a magnetic stirrer bar for 24 hrs prior to use. Each type of activating solution was prepared at a low-alkali concentration, with a 4% Na_2O to slag wt. ratio, and a high-alkali concentration, where 7% Na_2O was used in the ratio. Paste samples were prepared by mixing the slag with the designated solution for 2 minutes with mechanical stirring at 1500 rpm under laboratory conditions, using a water to slag wt. ratio of 0.44. The pastes were then left to cure for 1, 2, and 7 days in sealed plastic cuvettes before further testing.

Table 1: Oxide composition (wt. %) of slag determined by XRF.[19]

Slag Source	CaO	SiO_2	Al_2O_3	MgO	SO_3	Other
High-Mg	36.1	34.5	10.5	12.7	2.7	3.5
Low-Mg	42.5	34.5	11.7	7.3	1.7	2.3

The samples subjected to accelerated carbonation were first ground by hand in a mortar and pestle after the prescribed curing time. The samples were ground finely (tens to hundreds of microns) so that the effects of diffusion through a solid (i.e., transportation) were minimized, and therefore the quantitative tests performed in this study will be dominated by the reaction kinetics of carbonation. Accelerated carbonation was carried out in 5 and 100% CO_2 conditions. A CO_2 incubator was used for carbonation at 5% CO_2, with a relative humidity of 67% and a temperature of 29 °C. For carbonation at 100% CO_2, a custom carbonation chamber was set up to allow dry, industrial grade

CO_2 to flow over the sample with a low flow rate (<0.5 L/min) limited by a rotameter. The carbonation chamber was set up in a fume hood and remained at ambient temperature. Samples were exposed to 100% CO_2 for a duration of 24 hrs. Exposure of samples to 5% CO_2 was carried out for a range of exposure times, as reported in the Results and Discussion section.

Samples analyzed using X-ray diffraction were firstly loaded into 1 mm outer diameter polyimide capillaries, which were sealed at both ends with quick set epoxy. The capillaries were measured on a Bruker D8 Advance XRD with a silver X-ray tube ($K\alpha_1$ wavelength of 0.55941 Å, $K\alpha_2$ of 0.56380 Å). The samples were scanned from 3° to 30° 2θ with a step size of 0.007°, and a 5s count time per step. Phase identification was carried out using the Bruker Eva software and the IDCC PDF-2 database. XRD patterns have been converted from 2θ to Q-space for plotting, where $Q = 4\pi \sin\theta/\lambda$. Phase identification by XRD was carried out for all combinations of slag type, activator type and concentration, and curing time for accelerated carbonation in 100% CO_2. Additionally, low-alkali silicate activated slags (both high- and low-Mg) were analyzed using XRD after a curing time of 7 days followed by exposure to 5% CO_2 in the CO_2 incubator for up to 5 days.

Silicate-activated slag samples that were carbonated in 100% CO_2 were also analyzed using attenuated total reflectance Fourier Transform Infrared spectroscopy (ATR-FTIR). Samples were measured as powders using a Perkin Elmer Frontier FTIR instrument with a universal ATR sampling accessory. For each measurement the instrument was purged with N_2 gas to eliminate atmospheric H_2O and CO_2 contributions. 32 scans were taken for each sample, with a scan speed of 1 cm/s, a resolution of 4 cm^{-1} and the wavenumber ranging from 550 to 4000 cm^{-1}.

The extent of carbonation as a function of time was determined using thermogravimetric analysis (TGA) for the AAS samples (synthesized using high- and low-Mg slags) cured for 7 day followed by carbonation at 5% CO_2. This technique involved placing ~15 mg of the powder sample in a platinum pan which was heated to 950 °C in a Perkin Elmer Pyris 1 TGA instrument, using a 10 °C/min heating rate and an N_2 environment. TGA was also conducted on non-carbonated samples to determine the amount of binder gel prior to carbonation. FTIR analysis of the gaseous products released during a TGA run was carried out using a TL 8000 transfer line and an IR cell (Perkin

Elmer) mounted on the Frontier FTIR instrument. For the transfer line, a flow rate of 20 mL/min was used at a temperature of 300 °C. The IR cell was set at a temperature of 250 °C. The FTIR instrument was purged with N_2 to avoid atmospheric H_2O and CO_2 contributions. FTIR data were collected on the IR cell every 22 seconds for a single scan, using a scan speed of 1 cm/s, a resolution of 4 cm^{-1} and the wavenumber ranging from 550 to 4000 cm^{-1}.

Alkali Activation of Slag: Reaction Kinetics and Phase Formation

The XRD patterns of AAS at 1, 2 and 7 days prior to carbonation are depicted in Figures 1 to 4. These figures show that different types of slag (low- and high-Mg) and different activating solutions (silicate- and hydroxide-activated with 4% (low-alkali) or 7% (high-alkali) Na_2O) lead to slight variations in the formation kinetics and resulting reaction products. As seen in Figure 1, low-alkali silicate-activated high-Mg slag seems to activate slower than the equivalent low-Mg slag sample, specifically via the evolution of the main C-(N)-A-S-H gel peak at a Q value of ~2.1 $Å^{-1}$. After 1 day of curing by the low-alkali silicate solution, this peak is not apparent in the high-Mg slag (Figure 1b), while it has developed in the low-Mg slag (Figure 1a). This discrepancy demonstrates that this high-Mg slag activates slower in the activating solution (low-alkali silicate-activator) and has not formed sufficient C-(N)-A-S-H gel in the first 24 hrs to be detected by XRD. The particle size distribution of both types of slag were measured and found to be similar (Figure S1 in the Supplementary Material), so it is likely that the composition of the high-Mg slag leads to this lower reactivity. Specifically, via analysis of the slag basicity (using oxide wt. % and the equation $CaO+MgO/SiO_2$), it is found that the low-Mg slag has a higher basicity value (1.44) compared with the high-Mg slag (1.41), and both these slags have higher basicity values than the slags studied by Ben Haha *et al.*, where the behavior of the isothermal calorimetry data is aligned with the calculated basicity values of the corresponding slags.[23] Nevertheless, it is important to note that in this study, increasing the concentration of the silicate solution leads to faster formation kinetics, as seen by the C-(N)-A-S-H peak that develops by 24 hrs in the high-alkali silicate-activated high-Mg slag (Figure 3b, similar to the C-(N)-A-S-H peak in the high-alkali silicate-activated low-Mg slag in Figure 3a).

In agreement with previous studies, the most prominent secondary phase formed in the silicate-activated slags is a hydrotalcite-like LDH phase (see Figures 1 and 3).[4,5,17] The primary peak associated with this LDH, located at a Q value of ~0.8 $Å^{-1}$, appears as a relatively broad and low intensity peak for the silicate-activated slags, indicating that this phase may be weakly crystalline. The LDH peak increases in intensity from 1 to 7 days as it forms, and, as expected, appears to have a higher intensity in the activated high-Mg slag due to the greater availability of magnesium.[17]

Figure 2 shows the XRD patterns of low- and high-Mg slag activated with low-alkali sodium hydroxide. Compared to the silicate-activated slags, the hydroxide-activated slags have narrower and more intensely scattering C-(N)-A-S-H peaks, indicating that the gel may be more nanocrystalline in the hydroxide-activated samples (as directly visible from X-ray pair distribution functions)[30]. Furthermore, the low-alkali hydroxide-activated high-Mg slag XRD pattern contains discernible C-(N)-A-S-H gel peaks by 24 hrs, in contrast to the silicate-activated slags with the same Na_2O composition. The faster formation kinetics associated with hydroxide-activation is likely due to the higher pH of the sodium hydroxide solution compared with sodium silicate with the same Na_2O composition, and thus slag is initially more reactive in this environment.[5] The hydroxide-activated low-Mg slag (low- and high-alkali, Figures 2 and 4, respectively) also forms an additional crystalline phase consistent with calcium hemicarboaluminate, another LDH that tends to form in AAS systems synthesized using low-Mg slags.[31,32]

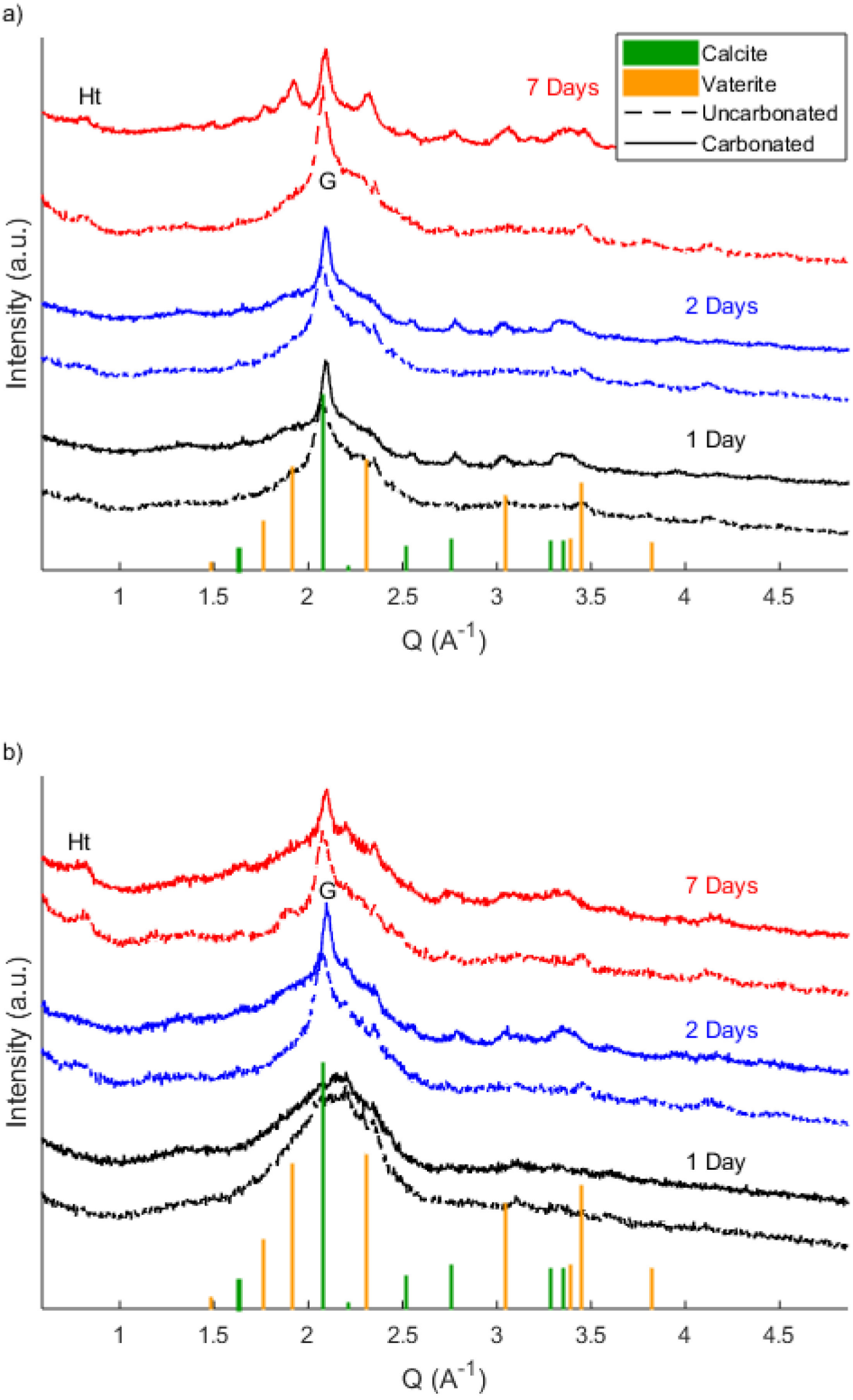

Figure 1: XRD patterns of low-alkali silicate-activated (a) low-Mg slag, and (b) high-Mg slag at 1, 2 and 7 days of curing, before and after carbonation in 100% CO_2 for 24 hrs. Ht denotes the hydrotalcite-like LDH phase while G denotes C-(N)-A-S-H gel.

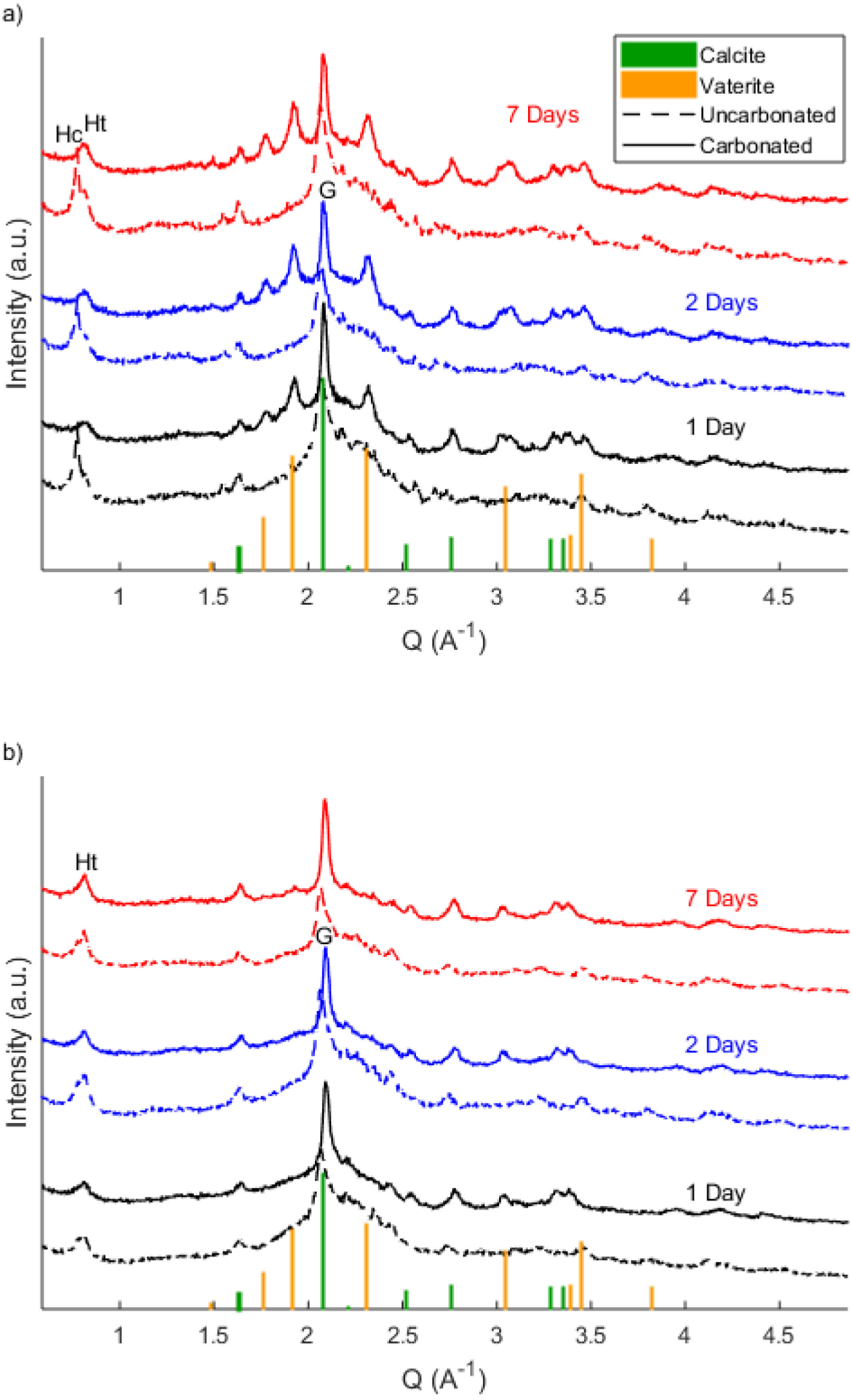

Figure 2: XRD patterns of low-alkali hydroxide-activated (a) low-Mg slag, and (b) high-Mg slag at 1, 2 and 7 days of curing, before and after carbonation in 100% CO_2 for 24 hrs. Ht denotes the hydrotalcite-like LDH phase, Hc the calcium hemicarboaluminate phase, while G denotes C-(N)-A-S-H gel.

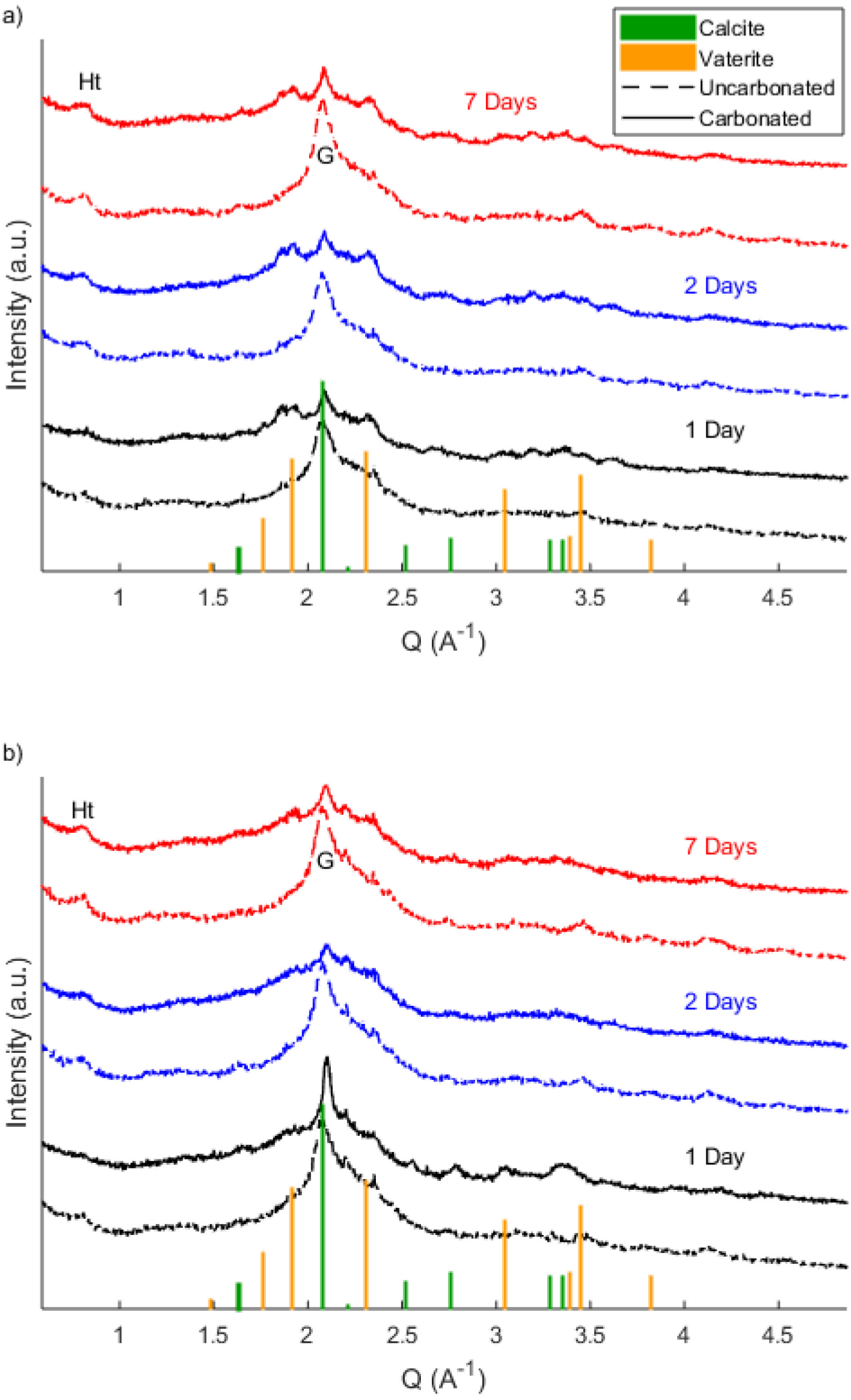

Figure 3: XRD patterns of high-alkali silicate-activated (a) low-Mg slag, and (b) high-Mg slag at 1, 2 and 7 days of curing, before and after carbonation in 100% CO_2 for 24 hrs. Ht denotes the hydrotalcite-like LDH phase while G denotes C-(N)-A-S-H gel.

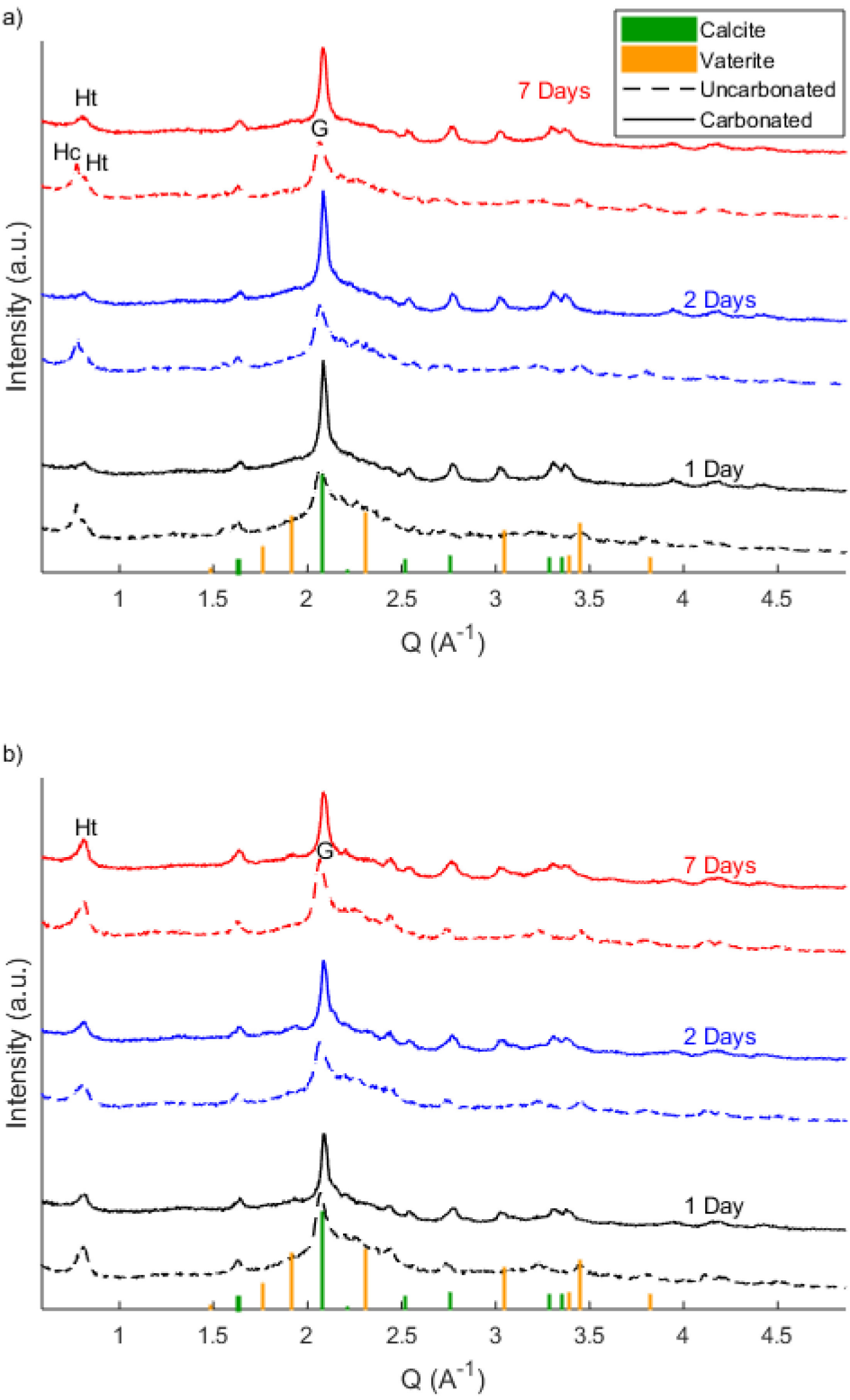

Figure 4: XRD patterns of high-alkali hydroxide-activated (a) low-Mg slag, and (b) high-Mg slag at 1, 2 and 7 days of curing, before and after carbonation in 100% CO_2 for 24 hrs. Ht denotes the hydrotalcite-like LDH phase, Hc the calcium hemicarboaluminate phase, while G denotes C-(N)-A-S-H gel.

Exposure to 100% CO_2: Impact of slag and activator chemistry

As mentioned in the Introduction, accelerated carbonation of AASs leads to calcium leaching from the C-(N)-A-S-H gel which then reacts with dissolved carbonate ions to form calcium carbonate, primarily the calcite and vaterite polymorphs.[16,27] Figures 1 through 4 show that the type of slag and activator, as well as the curing time, affect the calcium carbonate phases that form due to 100% CO_2 accelerated carbonation. Figure 1 displays the XRD patterns for low- and high-Mg slag activated with low-alkali silicate and carbonated in 100% CO_2, where calcite is the predominant crystalline phase that forms in the high-Mg slag samples (cured for 2 and 7 days in Figure 1b), while a significant amount of vaterite forms in the low-Mg sample carbonated after 7 days of curing (Figure 1a), which is consistent with previous studies.[17,27] The main calcite peak is located in the same *Q*-space region as the C-(N)-A-S-H gel peak, but is narrower and slightly shifted to higher scattering angles, while additional Bragg peaks of calcite are also apparent at higher *Q* values, as seen in Figures 1a and 1b. The low-Mg slag forms vaterite only after curing for seven days, and therefore the curing age as well as slag chemical composition have an impact on which calcium carbonate polymorphs form during carbonation. Finally, the high-Mg sample that did not form a detectible gel phase after only one day of curing (Figure 1b) does not form a crystalline calcium carbonate phase after exposure to 100% CO_2. Table 2 summarizes these findings for low- and high-Mg slag activated with low-alkali silicate (XRD data shown in Figure 1) together with the behavior of the other samples depicted in Figures 2, 3 and 4.

Table 2: Summary of calcium carbonate phases formed during carbonation of AAS in 100% CO_2 (24 hrs of exposure) based on (i) curing time, (ii) activator type and concentration and (iii) magnesium content of slag. C – Calcite, V – Vaterite, Am – amorphous.

Curing time (days)	**Low-Mg slag**			
	Silicate-activated		*Hydroxide-activated*	
	4% Na_2O	*7% Na_2O*	*4% Na_2O*	*7% Na_2O*
1	C	C + V, near Am	C + V	C
2	C	C + V, near Am	C + V	C
7	C + V	C + V, near Am	C + V	C
	High-Mg slag			
	Silicate-activated		*Hydroxide-activated*	
	4% Na_2O	*7% Na_2O*	*4% Na_2O*	*7% Na_2O*
1	Am	C	C	C
2	C	C, near Am	C	C
7	C	C, near Am	C	C

When the concentration of the sodium silicate activation solution is increased (Figure 3) the polymorphs of the calcium carbonate crystalline phases remain the same, however, their amounts change. The Bragg peaks attributed to the crystalline calcium carbonate polymorphs are broader and weaker in Figure 3 compared with Figure 1 (for the low-alkali silicate systems), indicating that the increased activator concentration has suppressed the formation of crystalline carbonation products, potentially due to the formation of ACC. However, crystalline calcite is seen to form after 1 day of curing in Figure 3b, which contrasts with a previous investigation that showed no formation of calcite or vaterite in the high-Mg silicate-activated slag when carbonated *in situ* with pure CO_2.[19] The *ex situ* nature of the current study may explain this difference, since an ACC could be forming *in situ* but then crystallizes into calcite when exposed to atmospheric conditions (during capillary loading) prior to *ex situ* characterization using XRD. Nevertheless, the lower crystallinity of calcium carbonate in the high-alkali silicate-activated slag compared with the low-alkali system may be caused by the high concentration of silicate ions in the initial activator, where the

subsequent pore solution composition (high silicate concentration) possibility disrupts crystallization of calcium carbonate as will be discussed in more detail later.[33]

The impact of activator concentration on the carbonation process for high-Mg silicate-activated slag has also been investigated using FTIR, where the results are shown in Figure 5. The low-alkali silicate sample, which did not show crystalline calcite in the XRD after one day of curing (Figure 1b), does still show a change when carbonation occurs. In particular, the carbonate out-of-plane bending mode at 865 cm^{-1} and the anti-symmetric stretching at ~1400 cm^{-1} emerge after carbonation, indicating that some form of carbonate still forms, even if it is not crystalline calcite.[14,34,35] This carbonate phase appears to be amorphous, as the peak at 865 cm^{-1} is broad in comparison to the peak from the crystallized calcite in the high-alkali silicate sample.[36] Furthermore, unlike the low-alkali sample, the high-alkali sample in Figure 5 shows a strong shift in the Si-O-T peak from 947 cm^{-1} to 1003 cm^{-1} (T denotes tetrahedral silica and alumina), consistent with high degrees of polymerization of the (alumino)silica gel that forms via decalcification of C-(N)-A-S-H gel.[37]

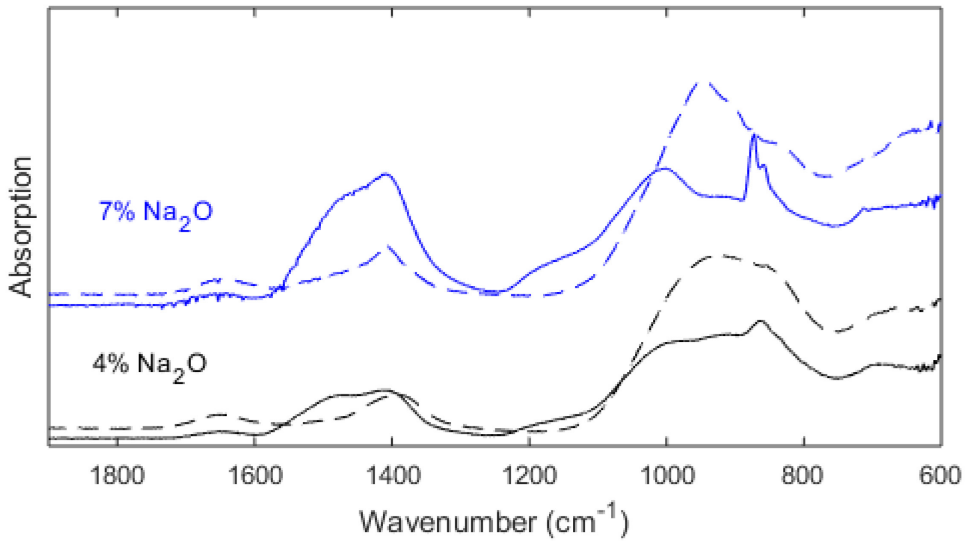

Figure 5: FTIR spectra of low- and high-alkali high-Mg silicate-activated slag pastes cured for 1 day followed by exposure to 100% CO_2 for 24 hrs. Before carbonation is shown by the dashed curves, and after carbonation by the solid curves.

The slags activated with sodium hydroxide are seen to behave differently from sodium silicate-activated slags when subjected to 100% CO_2 conditions. Specifically, carbonation of hydroxide-activated slags (both low- and high-Mg slag) lead to the precipitation of more crystalline calcium carbonate phases (narrower and more intense Bragg peaks in Figures 2 and 4) compared with silicate-activated slags (Figures 1 and 3). As was the case for the low-alkali silicate-activated samples, the low-alkali hydroxide-activated samples form specific crystalline calcium carbonate phases according to the magnesium concentration of the slag, where low-Mg slag forms vaterite and calcite while high-Mg slag only form calcite (see Table 2). However, when the concentration of the hydroxide is increased (i.e., high-alkali samples), both types of slag form only calcite, with no detectible amount of vaterite. Hence, the higher activator concentration for hydroxide activation leads to the formation of the most stable calcium carbonate polymorph, crystalline calcite, while increasing the concentration of the silicate activator favors less crystalline, and therefore less stable, calcium carbonate phases. However, from the XRD data in this investigation it is difficult to ascertain the amount of carbonation that has occurred. This aspect of the AAS carbonation will be assessed below using TGA data for samples exposed to 5% CO_2. Finally, it is noted that in all hydroxide-activated samples, the calcium hemicarboaluminate phase that forms during curing disappears from the diffraction pattern after carbonation (Figures 2 and 4). This LDH phase appears to be unstable and reacts readily with carbon dioxide.

Exposure to 5% CO_2

Magnesium Incorporation in Calcite

Figure 6 shows that both the high- and low-Mg slags activated using low-alkali sodium silicate form calcite and vaterite when subjected to moderate accelerated carbonation conditions (5% CO_2, 67% relative humidity). For the high-Mg sample (Figure 6b), the locations of the calcite peaks shift to larger Q values than the literature suggests for pure calcite.[38] For example, the most prominent calcite peak, the [1 0 4] reflection, occurs at 2.076 $Å^{-1}$ in the high-Mg sample, while this reflection occurs at 2.068 $Å^{-1}$ in the literature (shift of 0.008 $Å^{-1}$ which corresponds to a shift in *d*-spacing of ~0.01 Å). It appears that the greater availability of magnesium in this AAS leads to incorporation of magnesium ions in the calcite unit cell. Since magnesium ions are small than calcium ions, this leads to contraction of the unit cell and the observed peak shifts.[38] A qualitative assessment of the extent of magnesium incorporation in calcite can be carried out by comparison of the unit cell volume calculated from the XRD peak locations, with greater incorporation of magnesium leading to a more contracted unit cell. The unit cell parameters *a* and *c* of calcite (hexagonal) have been fit to equation 1 with a least-squares regression simultaneously using the *d*-spacings of four or five Bragg's peaks from calcite along with their known *h, k, l* reflections.

$$\frac{1}{d^2} = \frac{4}{3}\frac{h^2 + hk + k^2}{a^2} + \frac{l^2}{c^2} \qquad (1)$$

The unit cell volume of calcite as a function of slag MgO content and carbonation time is plotted in Figure 7, where the individual fit results are given (i.e., the volume obtained from the *a* and *c* parameters for a sample) along with the average unit cell volume for a given composition. For the low-Mg AAS, the calcite unit cell has a volume consistent with the reference (pure) calcite from the literature,[38] while the high-Mg AAS has a contracted calcite unit cell volume. Hence, this contraction of the calcite unit cell for the high-Mg AAS sample is likely caused by the incorporation of magnesium.[19,29] Given that magnesium is seen to be incorporated into calcite, it is highly like that it is incorporated into other calcium carbonate polymorphs. When incorporated into ACC, magnesium can have a stabilizing effect preventing crystallization and thus improving carbonation resistance, as previously mentioned.

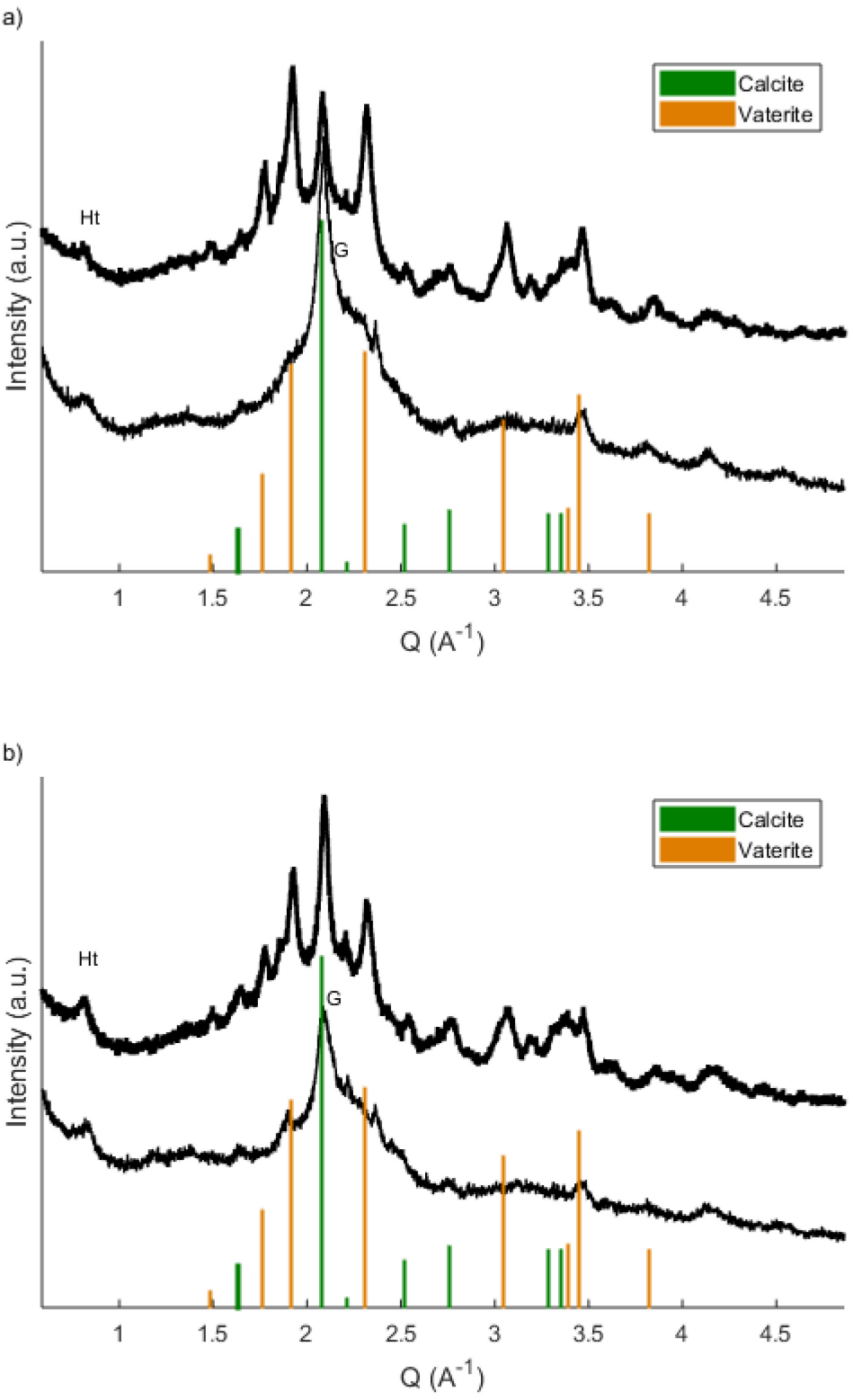

Figure 6: Low-alkali silicate-activated (a) low-Mg and (b) high-Mg slag after 7 days of curing, before and after carbonation in 5% CO_2 for 24 hrs (upper curve).

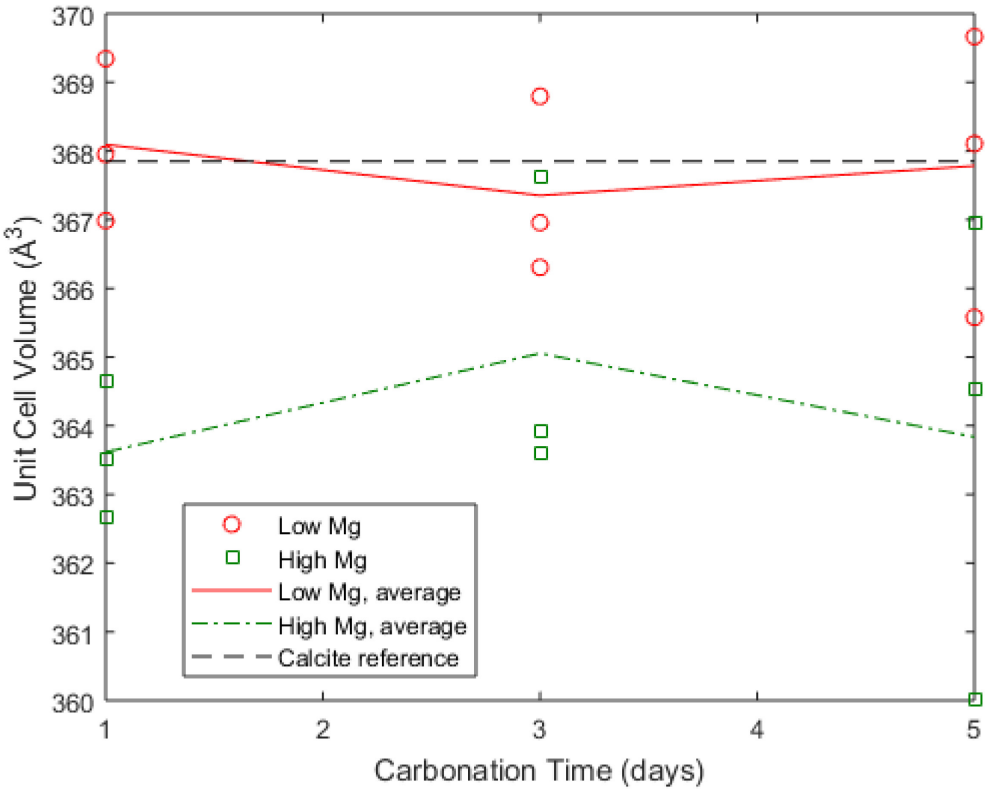

Figure 7: Unit cell volume of calcite in low-alkali silicate-activated slags (low- and high-Mg slags) that were subjected to 5% CO_2 for the designated carbonation time after 7 days of curing. Each marker in the figure is for a given sample while the lines were obtained by taking the average of the samples. The reference unit cell volume for calcium is from literature.[38]

Kinetics of CO_2 Uptake

So far, this investigation has shown that phase formation in AAS due to carbonation in a 100% CO_2 environment is dependent on a number of factors, including activator type and activator concentration. Furthermore, the ability for magnesium to be incorporated into calcium carbonate phases (specifically calcite) has been assessed using XRD and quantification of Bragg peak locations. In this section, TGA is used to quantify the amount of CO_2 that reacts with AAS during carbonation.

The TGA curves for low-alkali AAS samples cured for 7 days before and after carbonation are shown in Figure 8 together with their derivative curves (DTG). For the non-carbonated samples, they all lose the most weight from the start of the measurement until around 200 °C, which corresponds to water lost from the pore space as well as dehydration of the reaction product, C-

(N)-A-S-H gel.[5] These samples also show peaks in the DTG curves around 300 to 400 °C (see Figure 8b) which are consistent with loss of hydroxyl units and carbonates from the decomposition of the hydrotalcite-like LDH.[5,39,40]

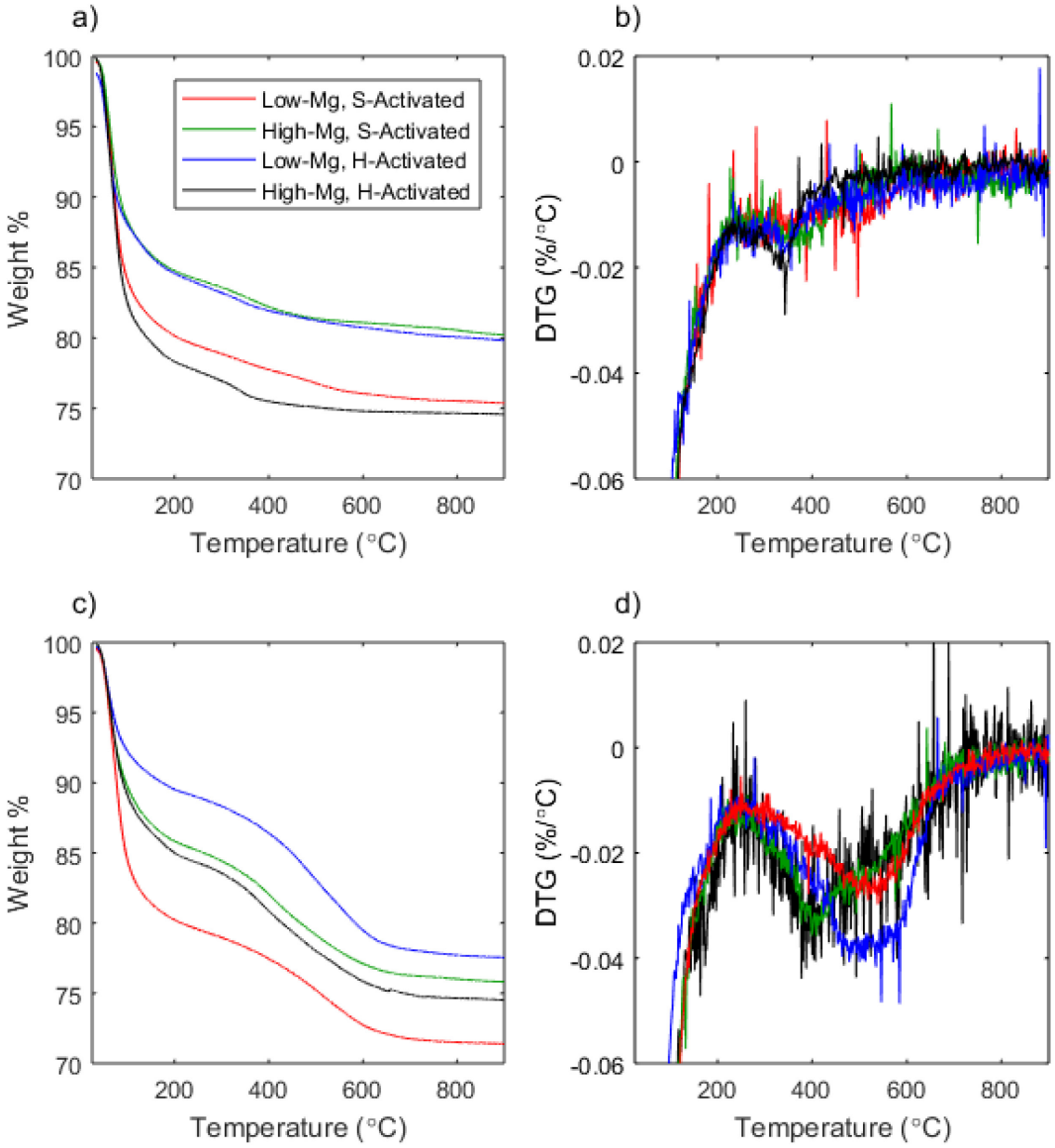

Figure 8: Example weight loss curves as a function of temperature and their derivatives (DTG) obtained using TGA for low-alkali AAS cured for 7 days. (a) and (b) are the TGA and DTG curves, respectively, for samples before carbonation, and (c) and (d) are the TGA and DTG curves, respectively, for samples carbonated for 1 hr in 5% CO_2. Note that plotting of the DTG curves has been carried out to focus on the hydrotalcite-like phase in the samples before carbonation, and the carbonate-containing phases after carbonation. See Figure S2 in the Supplementary Material for the corresponding DTG curves for samples carbonated for 24 hr in 5% CO_2.

After carbonation, the TGA data show a shift in weight loss to higher temperatures compared to the non-carbonated AAS (Figure 8). Calcium carbonate, in the form of calcite or other polymorphs, is expected to decompose into gaseous CO_2 and solid calcium oxide between 500 °C and 750 °C.[34,41] Figure 8b shows that the carbonated samples lose CO_2 over a temperature range of 245 °C to 710 °C (confirmed by FTIR analysis of the gaseous products, see Figures S3 and S4 in Supplementary Material for details). This CO_2 loss beginning at such low temperatures compared to expected values for calcium carbonate decomposition suggests that the hydrotalcite-like LDH phase has adsorbed a significant amount of CO_2 during the carbonation process.[21,42] The lower temperature weight loss can also be from desorption of CO_2 from other porous phases left after carbonation, such as the decalcified alumino-silicate gel. Comparing the DTG data (Figures 8d and S2) for the two silicate-activated slag samples, the low-Mg AAS has a narrower DTG peak at around 500 °C, while the high-Mg AAS has a broader peak that reaches maximum weight loss rate as low as 400 °C. Previous studies have shown that in carbonated AAS, the lower temperature weight loss corresponds to decomposition of the hydrotalcite-like LDH phase, while the higher temperature peak is due to the decomposition of calcium carbonate.[14,15] Since the overall CO_2 weight loss peak is a combination of these two decomposition events, it can be qualitatively evaluated that for the silicate-activated slag, a greater portion of the CO_2 weight loss in the high-Mg slag can be attributed to LDH desorption compared to the low-Mg slag.

Figure 9 shows the total weight of CO_2 captured by the AAS samples (calculated by subtracting sample weights at 245 °C and 710 °C) as a function of carbonation time, normalized to the sample weight at 710 °C. This normalization is useful because for a given activator and slag combination, the composition of the dry components remaining after 710 °C is roughly the same independent of the amount of water and CO_2 present in the sample before the TGA run was started. Over the first 24 hrs of carbonation in Figure 9a, the low-Mg silicate AAS carbonates the fastest, the high-Mg silicate AAS the slowest, and both the hydroxide-activated slags at about the same rate. Over an extended carbonation time up to 7 days, the trend continues with the high-Mg AAS taking up less CO_2 and at a slower rate compared with low-Mg AAS. Thus, for silicate-activated slag, a higher magnesium concentration quantifiably resists carbonation by reducing the rate of gel decalcification, and, as shown previously for 100% CO_2 conditions[43], also the total extent of gel

decalcification. These reductions in the silicate-activated high-Mg slag are a result of a reduced driving force responsible for the removal of calcium ions from C-(N)-A-S-H gel, specifically due to an elevated calcium concentration in the pore solution compared with silicate-activated low-Mg slag during exposure to CO_2. This elevated calcium concentration in the silicate-activated high-Mg slag system is caused by the prevalence of amorphous/low-crystallinity calcium carbonate phases in contrast to the crystalline calcium carbonates in silicate-activated low-Mg slag (as seen in XRD data in Figure 1 for samples exposed to 100% CO_2 and in Figure 6 for 5% CO_2). However, in the hydroxide-activated slag pastes the opposite trend is seen, where a greater extent of carbonation is observed for the high-Mg sample. Hence, it is likely that the propensity for decalcification to occur is also controlled by the availability of silicate ions in the pore solution. Previous research has revealed that silicate-activated slag has a higher silicon concentration in the pore solution (on the order of 10,000 ppm) compared with hydroxide-activated slag (on the order of 100 ppm) throughout the alkali-activation reaction (data from 1 day to 160 days).[44] Furthermore, previous research on the synthesis of ACC has shown that silica has a stabilizing effect on metastable ACC. Specifically, Kellermeier *et al.* explained that silica is coating the nanosized ACC, thereby limiting the ability of ACC to transform into crystalline polymorphs.[45] At room temperature and moderate silica concentrations (~5000 ppm), ACC is not sufficiently stabilized by the silica, and therefore crystallization readily occurs.[33] Hence, the mechanism controlling carbonation resistance of high-Mg alkali-activated slag appears to be more complex than first thought, where the availability of both magnesium and silica are important for obtaining a higher carbonation resistance paste when exposed to accelerated carbonation conditions ($\geq$ 5% CO_2), specifically by stabilization of the more soluble ACC phase compared with the lower solubility crystalline calcium carbonate phase.

Previous research has reported the positive effects of high alkali dosage (8 wt. % Na_2O relative to slag) and silicate modulus (activator SiO_2/Na_2O molar ratio of 2) on the short-term carbonation resistance of alkali-activated slag (under accelerated conditions, after 7 days of exposure to 3% CO_2 at 65% RH and 20 °C), attributing this positive behavior to the lower porosity and smaller average pore size of the mortars that were characterized.[46] However, in addition to these positive impacts on the pore structure, it cannot be discounted that the silicate oligomers associated with a high silicate modulus also augment the carbonation mechanism via stabilization of the ACC phase

during exposure to CO_2. The use of powder samples in this investigation enabled the separation of transport processes from the CO_2-induced chemical reactions.

In both silicate- and hydroxide-activated slags, the higher magnesium content allows for greater adsorption of CO_2 (adsorption on surfaces and in the hydrotalcite-like LDH phase) as evidenced by the more noticeable peaks in the DTG curves at ~400 °C in Figure 8b. Thus, the magnesium-containing LDH phase that forms in these AAS systems plays a noticeable role in CO_2 uptake by AAS, as identified by Bernal *et al.*[17] Although the LDH was not directly quantified in the current study, the greater availability of magnesium allows for greater amounts of this stable LDH to form[17] (in contrast to the calcium hemicarboaluminate phase that disappears on carbonation), which, in turn, will lead to a greater amount of CO_2 adsorption (separate from CO_2 absorption via gel decalcification and formation of calcium carbonate phases). What is unclear is whether there is a mechanistic link between the extent of hydrotalcite-like LDH CO_2 adsorption and a reduction in the extent of gel decalcification, as opposed to a correlation without causation. Here, we believe that the two processes are independent of each other, however, additional research is required in this domain.

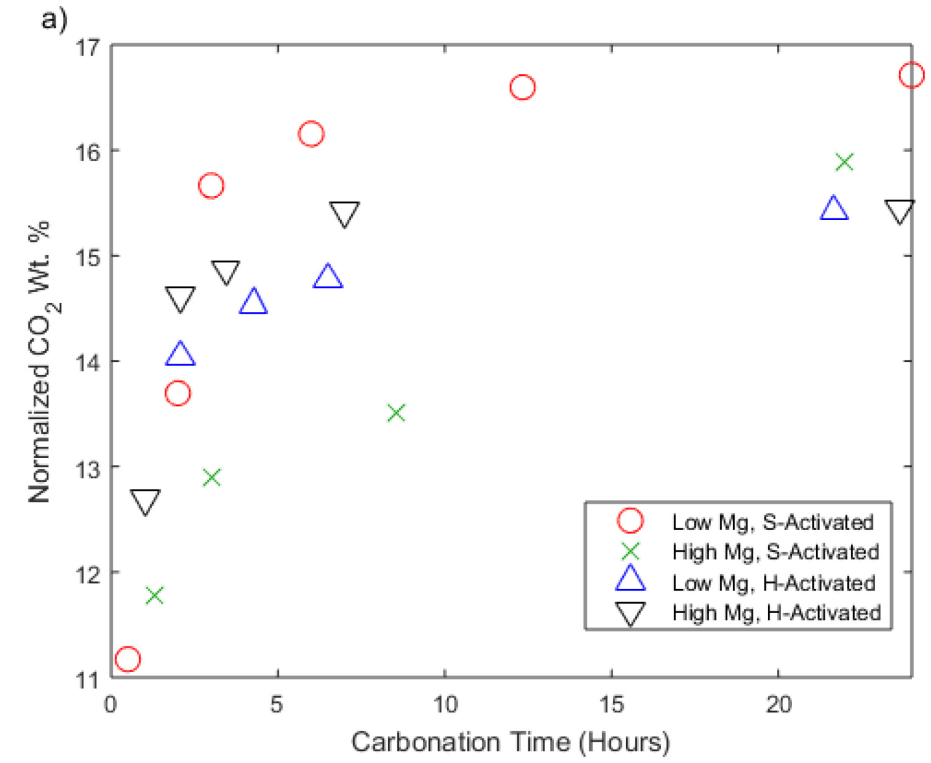

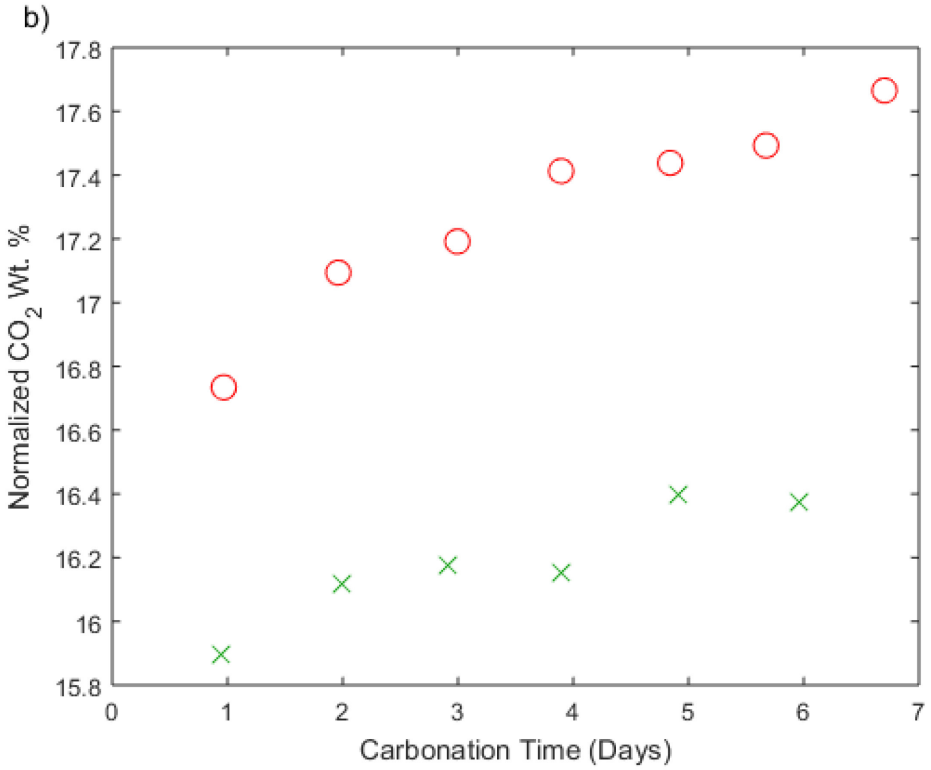

Figure 9: Total weight percent lost over temperature range from 245 to 710 °C (relative to dry weight at 710 °C) in low-alkali AASs versus exposure time in 5% CO_2 after a curing duration of 7 days. Carbonation time ranges up to (a) 24 hours and (b) 7 days.

Conclusions

In this study, alkali-activated slag (AAS) has been investigated under a range of accelerated carbonation conditions (5 and 100% CO_2), with the aim of uncovering the main factors controlling the extent of decalcification of the sodium-containing calcium-alumino-silicate-hydrate (C-(N)-A-S-H) gel. The influence of activator concentration (4 and 7 wt. % Na_2O relative to slag) activator type (hydroxide- and silicate-activator), slag MgO content (7 and 13 wt. %) and curing time on the carbonation resistance were explored on powder samples using X-ray diffraction (XRD), attenuated total reflectance – Fourier transform infrared (ATR-FTIR) spectroscopy, thermogravimetric analysis (TGA) and FTIR-TGA (for analysis of the gaseous products during heating). When samples were exposed to dry 100% CO_2 it was found that the higher activator concentration (7 wt. % Na_2O) combined with silicate activation led to less extensive formation of crystalline calcium carbonate phases. Furthermore, calcite was the only crystalline calcium carbonate seen to form in carbonated high-Mg AAS pastes while calcite and vaterite were observed in most carbonated low-Mg AAS pastes. TGA quantification of carbonated AAS revealed that for silicate-activated slags, the high-Mg slag sample was associated with a lower extent of CO_2 uptake and a slower rate of carbonation compared to the low-Mg slag sample. Moreover, a greater portion of the CO_2 was attributed to adsorption to phases like LDH for the high-Mg slag sample. The low-Mg silicate-activated slag sample was seen to have a greater portion of CO_2 associated with calcium carbonate, which, along with the greater total CO_2 uptake, implies a greater extent of decalcification of the C-(N)-A-S-H gel. Hence, these findings reveal that the chemical properties of both the slag and the activating solution affect the behavior of AAS when exposed to elevated CO_2 concentrations (5 and 100% CO_2).

An updated mechanism responsible for elevated carbonation resistance of alkali-activated high-Mg slag has been proposed in this study. Specifically, incorporation of both magnesium and silica in calcium carbonate appear to stabilize the ACC phase that initially forms on exposure to CO_2. The stabilization of this phase means that the equilibrium concentration of calcium ions in the pore solution is higher compared with the concentration for an equivalent system where calcite or calcite and vaterite (i.e., crystalline calcium carbonate phases) are prevalent. This higher concentration then leads to a lower driving force for C-(N)-A-S-H gel decalcification during carbonation. Hence, for applications where resistance to accelerated carbonation is desired, such as carbon

sequestration or oil well cements, a high magnesium content slag alone may not be enough to limit gel decalcification, since the appropriate activator must also be considered including the availability of silicate ions or other entities that are known to help stabilize ACC.

Acknowledgments

This research was supported by a National Science Foundation grant, No. 1553607. The authors acknowledge the use of Princeton's Imaging and Analysis Center, which is partially supported by the Princeton Center for Complex Materials, a National Science Foundation (NSF)-MRSEC program (DMR-1420541).

Supplementary Material

Particle size distribution of neat slags; Zoom of example derivative TGA curves (DTG curves); Analysis of gaseous products during TGA measurement. Supplementary Material associated with this article can be found in the online version.

References

1. Scrivener KL, Kirkpatrick RJ. Innovation in Use and Research on Cementitious Material. *Cem Concr Res*. 2008;38(2):128-136. doi:10.1016/j.cemconres.2007.09.025

2. Le Quéré C, Andrew RM, Canadell JG, et al. Global Carbon Budget 2016. *Earth Syst Sci Data*. 2016;8(2):605-649. doi:10.5194/essd-8-605-2016

3. Provis JL, van Deventer JSJ. *Alkali Activated Materials*. New York: Springer US; 2014. doi:10.1007/978-94-007-7672-2

4. Burciaga-Diaz O, Escalante-Garcia JI. Structure, Mechanisms of Reaction, and Strength of an Alkali-Activated Blast-Furnace Slag. *J Am Ceram Soc*. 2013;96(12):3939-3948. doi:10.1111/jace.12620

5. Ben Haha M, Le Saout G, Winnefeld F, Lothenbach B. Influence of Activator Type on Hydration Kinetics, Hydrate Assemblage and Microstructural Development of Alkali Activated Blast-Furnace Slags. *Cem Concr Res*. 2011;41(3):301-310. doi:10.1016/j.cemconres.2010.11.016

6. Bernal SA, Mejía De Gutiérrez R, Pedraza AL, Provis JL, Rodriguez ED, Delvasto S. Effect of Binder Content on the Performance of Alkali-Activated Slag Concretes. *Cem Concr Res*. 2011;41(1):1-8. doi:10.1016/j.cemconres.2010.08.017

7. Provis JL, Palomo A, Shi C. Advances in Understanding Alkali-Activated Materials. *Cem Concr Res*. 2015;78:110-125. doi:10.1016/j.cemconres.2015.04.013

8. Duxson P, Provis JL, Lukey GC, Mallicoat SW, Kriven WM, van Deventer JSJ. Understanding the Relationship Between Geopolymer Composition, Microstructure and Mechanical Properties. *Colloids Surfaces A Physicochem Eng Asp*. 2005;269(1-3):47-58. doi:10.1016/j.colsurfa.2005.06.060

9. Fernández-Jiménez A, Palomo A, Criado M. Microstructure Development of Alkali-Activated Fly Ash Cement: A Descriptive Model. *Cem Concr Res*. 2005;35(6):1204-1209. doi:10.1016/j.cemconres.2004.08.021

10. Neville AM. *Properties of Concrete*. 5th ed. London: Pearson; 2011.

11. Alonso C, Andrade C, González JA. Relation between Resistivity and Corrosion Rate of Reinforcements in Carbonated Mortar Made with Several Cement Types. *Cem Concr Res*. 1988;18(5):687-698. doi:10.1016/0008-8846(88)90091-9

12. Glasser FP, Marchand J, Samson E. Durability of Concrete - Degradation Phenomena Involving Detrimental Chemical Reactions. *Cem Concr Res*. 2008;38(2):226-246. doi:10.1016/j.cemconres.2007.09.015

13. Bernal SA, de Gutierrez RM, Provis JL, Rose V. Effect of Silicate Modulus and Metakaolin Incorporation on the Carbonation of Alkali Silicate-Activated Slags. *Cem Concr Res*. 2010;40(6):898-907. doi:10.1016/j.cemconres.2010.02.003

14. Li N, Farzadnia N, Shi C. Microstructural Changes in Alkali-Activated Slag Mortars Induced by Accelerated Carbonation. *Cem Concr Res*. 2017;100(2):214-226. doi:10.1016/j.cemconres.2017.07.008

15. Palacios M, Puertas F. Effect of Carbonation on Alkali-Activated Slag Paste. *J Am Ceram Soc*. 2006;89(10):3211-3221. doi:10.1111/j.1551-2916.2006.01214.x

16. Bernal SA, Provis JL, Brice DG, Kilcullen A, Duxson P, van Deventer JSJ. Accelerated Carbonation Testing of Alkali-Activated Binders Significantly Underestimates Service Life : The Role of Pore Solution Chemistry. *Cem Concr Res*. 2012;42(10):1317-1326. doi:10.1016/j.cemconres.2012.07.002

17. Bernal SA, San R, Myers RJ, et al. MgO Content of Slag Controls Phase Evolution and Structural Changes Induced by Accelerated Carbonation in Alkali-Activated Binders. *Cem Concr Res*. 2014;57:33-43. doi:10.1016/j.cemconres.2013.12.003

18. Khan MSH, Castel A. Effect of MgO and Na_2SiO_3 on the Carbonation Resistance of Alkali Activated Slag Concrete. *Mag Concr Res*. 2018;70(13):685-692. doi:10.1680/jmacr.17.00062

19. Morandeau AE, White CE. Role of Magnesium-Stabilized Amorphous Calcium Carbonate in Mitigating the Extent of Carbonation in Alkali-Activated Slag. *Chem Mater*. 2015;27:6625-6634. doi:10.1021/acs.chemmater.5b02382

20. Meyn M, Beneke K, Lagaly G. Anion-Exchange Reactions of Layered Double

Hydroxides. *Inorg Chem*. 1990;29(26):5201-5207. doi:10.1021/ic00351a013

21. Sahoo P, Ishihara S, Yamada K, et al. Rapid Exchange between Atmospheric CO_2 and Carbonate Anion Intercalated within Magnesium Rich Layered Double Hydroxide. *ACS Appl Mater Interfaces*. 2014;6:18352-18359.

22. Myers RJ, Lothenbach B, Bernal SA, Provis JL. Thermodynamic Modelling of Alkali-Activated Slag-Based Cements. *Appl Geochemistry*. 2015;61:233-247.

23. Ben Haha M, Lothenbach B, Saout G Le, Winnefeld F. Influence of Slag Chemistry on the Hydration of Alkali-Activated Blast-Furnace Slag — Part I : Effect of MgO. *Cem Concr Res*. 2011;41(9):955-963. doi:10.1016/j.cemconres.2011.05.002

24. Ben Haha M, Lothenbach B, Le Saout G, Winnefeld F. Influence of Slag Chemistry on the Hydration of Alkali-Activated Blast-Furnace slag - Part II: Effect of Al_2O_3. *Cem Concr Res*. 2012;42(1):74-83. doi:10.1016/j.cemconres.2011.08.005

25. Wang S-D, Scrivener KL, Pratt PL. Factors Affecting Strength of Alkali-Activated Slag. 1993;24(6):1033-1043. doi:10.1016/0008-8846(94)90026-4

26. Nasvi MCM, Ranjith PG, Sanjayan J. Effect of Different Mix Compositions on Apparent Carbon Dioxide (CO_2) Permeability of Geopolymer: Suitability as Well Cement for CO_2 Sequestration Wells. *Appl Energy*. 2014;114:939-948. doi:10.1016/j.apenergy.2013.05.050

27. Morandeau AE, White CE. In Situ X-Ray Pair Distribution Function Analysis of Accelerated Carbonation of a Synthetic Calcium-Silicate-Hydrate Gel. *J Mater Chem A*. 2015;3(16):8597-8605. doi:10.1039/c5ta00348b

28. Radha A V, Fernandez-martinez A, Hu Y, Jun Y, Waychunas GA, Navrotsky A. Energetic and Structural Studies of Amorphous Ca_{1-x} Mg_x CO_3 nH_2O ($0<x<1$). *Geochim Cosmochim Acta*. 2012;90:83-95. doi:10.1016/j.gca.2012.04.056

29. Loste E, Wilson RM, Seshadri R, Meldrum FC. The Role of Magnesium in Stabilising Amorphous Calcium Carbonate and Controlling Calcite Morphologies. *J Cryst Growth*. 2003;254(1-2):206-218. doi:10.1016/S0022-0248(03)01153-9

30. Garg N, Özçelik VO, Skibsted J, White CE. Nanoscale Ordering and Depolymerization of Calcium Silicate Hydrates in the Presence of Alkalis. *J Phys Chem C*. 2019;123(40):24873-24883. doi:10.1021/acs.jpcc.9b06412

31. Whittaker M, Zajac M, Ben Haha M, Bullerjahn F, Black L. The Role of the Alumina Content of Slag, Plus the Presence of Additional Sulfate on the Hydration and Microstructure of Portland Cement-Slag Blends. *Cem Concr Res*. 2014;66:91-101. doi:10.1016/j.cemconres.2014.07.018

32. Gong K, White CE. Nanoscale Chemical Degradation Mechanisms of Sulfate Attack in Alkali-activated Slag. *J Phys Chem C*. 2018;122(11):5992-6004. doi:10.1021/acs.jpcc.7b11270

33. Kellermeier M, Glaab F, Klein R, Melero-García E, Kunz W, García-Ruiz JM. The Effect of Silica on Polymorphic Precipitation of Calcium Carbonate: An On-line Energy-Dispersive X-Ray Diffraction (EDXRD) Study. *Nanoscale*. 2013;5(15):7054-7065. doi:10.1039/c3nr00301a

34. Ashraf W, Olek J. Carbonation Behavior of Hydraulic and Non-Hydraulic Calcium Silicates : Potential of Utilizing Low-Lime Calcium Silicates in Cement-Based Materials. *J Mater Sci*. 2016;51(13):6173-6191. doi:10.1007/s10853-016-9909-4

35. Lam RSK, Charnock JM, Lennie A, Meldrum FC. Synthesis-Dependent Structural Variations in Amorphous Calcium Carbonate. *CrystEngComm*. 2007;9(12):1226-1236. doi:10.1039/b710974a

36. Gebauer D, Gunawidjaja PN, Ko JYP, et al. Proto-Calcite and Proto-Vaterite in Amorphous Calcium Carbonates. *Angew Chemie Int Ed*. 2010;49:8889-8891. doi:10.1002/anie.201003220

37. Bernal SA, Provis JL, Walkley B, et al. Gel Nanostructure in Alkali-Activated Binders Based on Slag and Fly Ash, and Effects of Accelerated Carbonation. *Cem Concr Res*. 2013;53:127-144. doi:10.1016/j.cemconres.2013.06.007

38. Bischoff WD, Bishop FC, Mackenzie FT. Biogenically Produced Magnesian Calcite : Inhomogeneities and Physical Properties; Comparison with Synthetic Phases. *Am Mineral*.

1983;68:1183-1188.

39. Miyata S. Physico-Chemical Properties of Synthetic Hydrotalcites in Relation to Composition. *Clays Clay Miner*. 1980;28(1):50-56. doi:10.1346/CCMN.1980.0280107

40. Abdel-Gawwad HA, El-Aleem SABD. Effect of Reactive Magnesium Oxide on Properties of Alkali Activated Slag Geopolymer Cement Pastes. *Ceram - Silikaty*. 2015;59(1):37-47.

41. Villain G, Thiery M, Platret G. Measurement Methods of Carbonation Profiles in Concrete: Thermogravimetry, Chemical Analysis and Gammadensimetry. 2007;37:1182-1192. doi:10.1016/j.cemconres.2007.04.015

42. Rey F, Fornés V, Rojo JM. Thermal Decomposition of Hydrotalcites. An Infrared and Nuclear Magnetic Resonance Spectroscopic Study. *J Chem Soc Faraday Trans*. 1992;88(15):2233-2238. doi:10.1039/FT9928802233

43. Wang SY, McCaslin E, White CE. Effects of Magnesium Content and Carbonation on the Multiscale Pore Structure of Alkali-Activated Slags. *Cem Concr Res*. 2020;130:105979. doi:10.1016/j.cemconres.2020.105979

44. Puertas F, Fernández-Jiménez A, Blanco-Varela MT. Pore Solution in Alkali-Activated Slag Cement Pastes. Relation to the Composition and Structure of Calcium Silicate Hydrate. *Cem Concr Res*. 2004;34(1):139-148. doi:10.1016/S0008-8846(03)00254-0

45. Kellermeier M, Melero-García E, Glaab F, et al. Stabilization of amorphous Calcium Carbonate in Inorganic Silica-Rich Environments. *J Am Chem Soc*. 2010;132(50):17859-17866. doi:10.1021/ja106959p

46. Shi Z, Shi C, Wan S, Zhang Z. Effects of alkali dosage and silicate modulus on alkali-silica reaction in alkali-activated slag mortars. *Cem Concr Res*. 2018;111(July):104-115. doi:10.1016/j.cemconres.2018.06.005